TECHNICAL PAPER

Frequency-selective electrokinetic manipulation of microparticles in gold nanofilm optically-induced dielectrophoretic device

Yue-Chang Tsai[1] · Yong-Hang Hong[2] · Sheng-Jie Zhang[1] · Ju-Nan Kuo[1]

Abstract

A novel optically-induced dielectrophoretic (ODEP) device incorporating a gold nanofilm is proposed for the manipulation of microparticles. The electrokinetic phenomena induced under different optical radial images are investigated both numerically and experimentally. The results show that the gold nanofilm not only extends the operating frequency of the ODEP device, but also prompts a change in the direction of the DEP force from the outward direction to the inward direction at high frequencies. Consequently, particle concentration can be achieved in the high frequency range. Overall, the proposed device provides a bi-directional and velocity/force-controllable approach for the manipulation of microparticles in ODEP applications.

1 Introduction

The manipulation and separation of particles and cells is an essential step in the sample pretreatment and diagnosis procedures of many biomedical applications (Jager et al. 2000; Mello and Beard 2003); particularly those conducted in microfluidic systems. The literature thus contains many proposals for particle manipulation. For example, acoustic waves (Shi et al. 2009) can be used to induce the continuous separation of particles in a microfluidic channel via an acoustophoretic effect. However, in implementing such an approach, a tradeoff must be made between the resolution and the throughput. Optical tweezers (Grier 2003) provide a high-resolution approach for the manipulation of single cells or particles. However, the intense localized heating effect produced by the high optical power required to trap the particles may result in the damage of live cells. Furthermore, the complicated optical setup and expensive instrumentation increase the system cost, and hence further limit their practicality for microfluidics applications. Magnetic manipulation (Nguyen 2012) provides a feasible

approach for separating microparticles. However, it achieves a poor performance in separating particles with small size variations and degrees of magnetization. Furthermore, the high device temperature induced under large magnetic forces may damage biosamples. Consequently, the use of dielectrophoretic (DEP) devices to perform the relatively low-temperature manipulation and separation of particles in microfluidic channels has attracted significant interest in recent decades for a variety of applications, including trapping/sorting (Huang et al. 2003; Gascoyne and Vykoukal 2004; Grilli and Ferraro 2008), carbon nanotube separation/assembly (Krupke et al. 2003; Gennari et al. 2013), cell manipulation (Voldman 2006), self-assembling of liquid crystal and nanoparticles (Merola et al. 2012; Grilli et al. 2014), and quantum dots driven by pyroelectric-dielectrophoresis (Nasti et al. 2018). DEP is traditionally implemented by using a microelectrode and non-uniform alternating current (AC) electric field to induce the motion of polarized particles or cells. However, the fabrication process for conventional DEP devices usually requires complicated photolithography techniques and the use of delicate thin-film deposition and etching processes to pattern the microelectrodes (Pethig and Markx 1997).

Optoelectronic tweezers (OET), also known as optically-induced dielectrophoretic (ODEP) devices, manipulate the particles and cells using virtual electrodes produced by simple optical images (Chiou et al. 2005). As a result, they greatly simplify the fabrication process compared to

✉ Ju-Nan Kuo
   junan@nfu.edu.tw

1   Department of Automation Engineering, National Formosa
    University, No. 64, Wenhua Rd, Huwei 632, Yunlin, Taiwan

2   Department of Nutrition, I-Shou University, No. 8, Yida Rd,
    Jiaosu Village, Yanchao District, Kaohsiung City 824,
    Taiwan

conventional DEP devices with physical electrodes. In ODEP, the light image is projected onto a photoconductor material under an AC voltage, and the resulting non-uniform electric field distribution induces an ODEP force which acts on the particles. Due to the high photoconductive gain of amorphous silicon, a low optical intensity ($\sim 10^4$ W/m^2) is sufficient to activate the virtual electrode (Mishra et al. 2014). As a result, the operating temperature is significantly lower than that of traditional optical tweezers, and hence ODEP devices are more conducive to the manipulation of live cells and biosamples. Furthermore, each pixel of a liquid crystal display (Hwang et al. 2008), or computer projector (Lu et al. 2006), can be individually activated utilizing the ODEP method; resulting in the formation of hundreds or even thousands of ODEP traps. Consequently, ODEP provides the ability to dynamically create real-time, reconfigurable virtual electrodes and a DEP force over a large working area. It has thus attracted great interest for a wide variety of applications in recent years, including the separation of nanowires (Jamshidi et al. 2008) and cells (Hwang et al. 2009), the dynamic patterning of nanoparticles (Jamshidi et al. 2009; Muñoz-Martínez et al. 2017), immobilizing and orienting Escherichia coli bacteria (Miccio et al. 2016), and the sorting of cancer cells (Zhang et al. 2018; Chu et al. 2019).

A typical ODEP device consists of a transparent glass slide coated with indium tin oxide (ITO), a liquid layer containing the cells or particles to be manipulated, and a photoconductor substrate. The substrate typically comprises a thin layer of ITO doped with hydrogenated amorphous silicon (a-Si:H) deposited on a glass surface. Bulk-heterojunction polymers such as P3HT and PCBM can also be used as light active layers to perform cell/particle manipulation in ODEP devices (Wang et al. 2010). However, the associated fabrication process requires complex chemical handling and thermal deposition procedures. Using titanium oxide phthalocyanine (TiOPc), a photoconductive surface can be prepared in a single spin-coating step. However, the stability of the TiOPc film degrades over time (Yang et al. 2010). Various studies have shown that oxide crystal can also be used as the photoconductor substrate in ODEP devices (Esseling et al. 2012; Miccio et al. 2012). However, the response time and trapping process are typically slower than those in a-Si:H-based devices. Accordingly, the present study proposes the use of a gold nanofilm to enhance the electrokinetic manipulation ability of an ODEP device. The conduction current and absorption spectrum of the gold nanofilm are explored. In addition, the electrokinetic phenomena induced in the proposed device under different radial images are investigated both numerically and experimentally. The purpose of this paper is to demonstrate the use of a gold nanofilm ODEP device to induce a second frequency

crossover point at higher frequencies. In other words, the device provides both a negative DEP force (at lower frequencies) and a positive DEP force at higher frequencies. It is shown that the proposed device provides a promising approach for the frequency-selective electrokinetic manipulation of cells or particles in a variety of microfluidic applications.

2 Materials and methods

2.1 Experimental setup

A gold nanofilm ODEP microfluidic system was designed to provides a bi-directional and velocity/force-controllable approach for the manipulation of microparticles in ODEP applications. Figure 1 presents a schematic illustration of the proposed ODEP chip consisting of two ITO-coated glass plates (7 Ω, 0.7 mm; Ritek, Taiwan) separated by a thin liquid layer containing the microparticles to be manipulated. As shown, the lower glass substrate is coated with a thin (1-μm) a-Si:H layer deposited by plasma-enhanced chemical vapor deposition (PECVD), while the upper glass substrate is coated with a conductive gold nanofilm prepared using a benchtop sputtering system with high resolution thickness controller (Sputter Coater 108 Auto, Pentad Scientific Corporation, Taiwan), the thickness is measured to a resolution of 0.1 nm. The liquid layer (with a thickness of 100 μm) was fabricated by a combination of CNC machining and PDMS replica molding and was filled with de-ionized (DI) water and polystyrene particles with a size of 90 μm. The present study
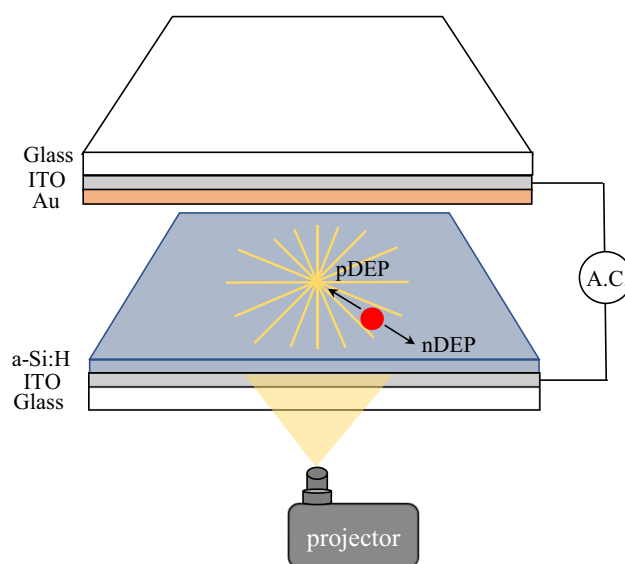

Fig. 1 Schematic illustration of selective manipulation of polystyrene particles by radial image projected onto ODEP chip

considered three projected optical images with 8-radial, 16-radial and 32-radial patterns, respectively. The width and length (radius) of the optical images are 20 μm and 1000 μm, for all three patterns. In performing the ODEP trials, radial optical images were projected onto the surface of the ODEP chip to form virtual electrodes and a particle manipulation force was produced using a function generator (Model 282, Fluke, USA) connected to an amplifier (Model 2100HF, Trek, USA). The resulting motion of the polystyrene particles was observed using a charge-coupled device (CCD)-equipped microscope (TrueChrome II, Tucsen, China). For example, as shown in the illustration of Fig. 1, particles can be manipulated by a radial image projected onto an ODEP chip. The particles are attracted to the center of the radial image since they experience a positive DEP force. By contrast, for a negative DEP force, the particles are pushed toward the outer region of the projected radial image.

2.2 The photoelectric characteristics of the gold nanofilm

Figure 2a shows the measured values of the conduction current for ITO-glass substrates coated with gold nanofilms with thicknesses ranging from $5 \sim 30$ nm. For a bare ITO glass substrate with no nanofilm, the conduction current is just 24 μA. However, the current increases to 35, 38, 46 and 50 μA for gold nanofilms with thicknesses of 5, 10, 20 and 30 nm, respectively. In other words, a significant improvement in the conduction current is obtained as the thickness of the gold nanofilm increases. Figure 2b shows the UV-NIR absorption spectra of the glass substrates with different gold nanofilm thicknesses, as measured by a commercial spectrometer (BRC112P-E, HMT, Taiwan). It is seen that in the visible light range (i.e., $380 \sim 760$ nm), green light (~ 500 nm) has the minimum absorption intensity in all five cases. For all of the substrates other than that coated with the thickest gold nanofilm (30 nm), the absorptivity increases after the red light region of the spectrum (~ 600 nm). The average absorptivity of the uncoated ITO glass substrate in the visible light range is around 15%. However, for the substrates coated with gold nanofilms with thicknesses of 5, 10, 20 and 30 nm, the average absorptivity increases to 42%, 59%, 76% and 92%, respectively. In other words, while a greater gold nanofilm thickness is beneficial in increasing the conduction current (see Fig. 2a), it results in an electrothermal effect and a lower optical transmission. Therefore, nanofilms with a thickness of 5 nm and 10 nm, respectively, were chosen as acceptable compromises between the conduction current and the optical transmittance for the ODEP chips used in the remainder of the study.

3 Numerical simulations

3.1 Theory

For a homogeneous dielectric spherical particle immersed in a conductive medium, the time-averaged DEP force can be expressed as (Hughes et al. 1996)

$$F_{DEP} = 2\pi a^3 \varepsilon_m \mathrm{Re}[CM] \nabla E^2, \tag{1}$$

where a is the radius of the particle, ε_m is the permittivity of the medium, $\mathrm{Re}[CM]$ is the real part of the complex Clausius–Mossotti (CM) factor, and E is the amplitude of the electric field. In other words, the DEP force (F_{DEP}) is proportional to the third power of the particle radius and the square of the applied electric field amplitude. The complex Clausius–Mossotti factor has the form

$$CM = \frac{\varepsilon_p^* - \varepsilon_m^*}{\varepsilon_p^* + 2\varepsilon_m^*}, \tag{2}$$

$$\varepsilon^* = \varepsilon - j\frac{\sigma}{\omega}, \tag{3}$$

where ε^* and σ are the complex permittivity and conductivity of the medium, respectively; subscripts p and m refer to the particle and medium, respectively; $\omega = 2\pi f$, where f is the frequency of the AC voltage applied across the liquid medium; and j is the imaginary unit. The DEP force acting on the particle may be either positive or negative, depending on the sign of the real part of the CM factor. For a positive DEP force (see Fig. 1, for example), the particles are attracted to the center of the radial image (i.e., the region of high electric field strength) and hence undergo a concentration effect. By contrast, for a negative DEP force, the particles are pushed toward the outer region of the projected radial image and undergo a separation effect.

3.2 Numerical characterization

As shown in Fig. 3, the present study considered three projected optical images with 8-radial, 16-radial and 32-radial patterns, respectively. For each image, the electrokinetic phenomena induced in the ODEP chip were examined numerically by COMSOL Multiphysics simulations (COMSOL Inc., USA). In performing the simulations, the physical and electrical properties of the conductive fluid (DI water) and particles (polystyrene beads) were specified as follows: $\rho_m = 1000$ kg/m³, $\rho_p = 1009$ kg/m³, $\varepsilon_m = 80$, $\varepsilon_p = 2.5$, $\sigma_m = 0.005$ S/m, and $\sigma_p = 0.0009$ S/m (Chiou et al. 2013, 2016). Furthermore, the amplitude and driving frequency of the AC electric field applied between the two ITO glass substrates were set as 20 V_{PP} and 300 Hz, respectively.

Fig. 2 Measurement results for ITO glass substrates with different gold nanofilm thicknesses: **a** conduction currents, and **b** UV–NIR absorption spectra
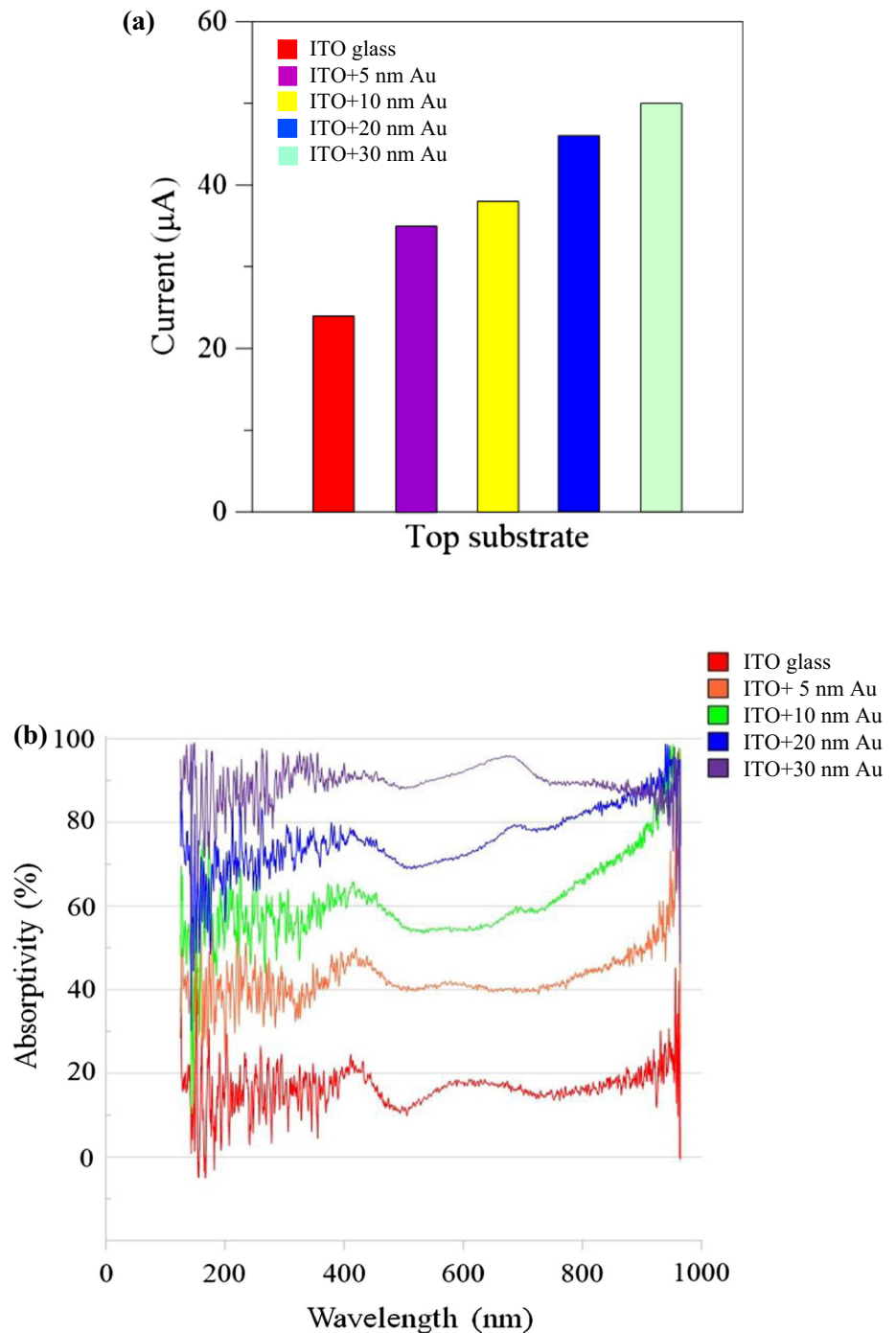
Referring to Fig. 3a, it is seen that a non-uniform electric field is formed at the optical virtual electrodes for every projected pattern. Moreover, the maximum electric field occurs at the center of each pattern and increases with an increasing number of virtual electrodes. From inspection, the maximum electric field reaches a value of 2.69×10^6 V/m at the center of the 32-radial pattern by numerical simulations. For all three patterns, the electric field gradient between the virtual electrodes is highly non-

uniform in the circumferential direction. Therefore, the particles not only are attracted to the radial direction of the projected patterns, but also induce a moving in the circumferential direction, and resulting in the velocity of the particles are affected. The non-uniformity is particularly apparent in the pattern with 8 radial electrodes and is thus not suitable for particle velocity analysis.

Figure 3b shows the simulation results for the variation of the electric field intensity in the radial direction of the
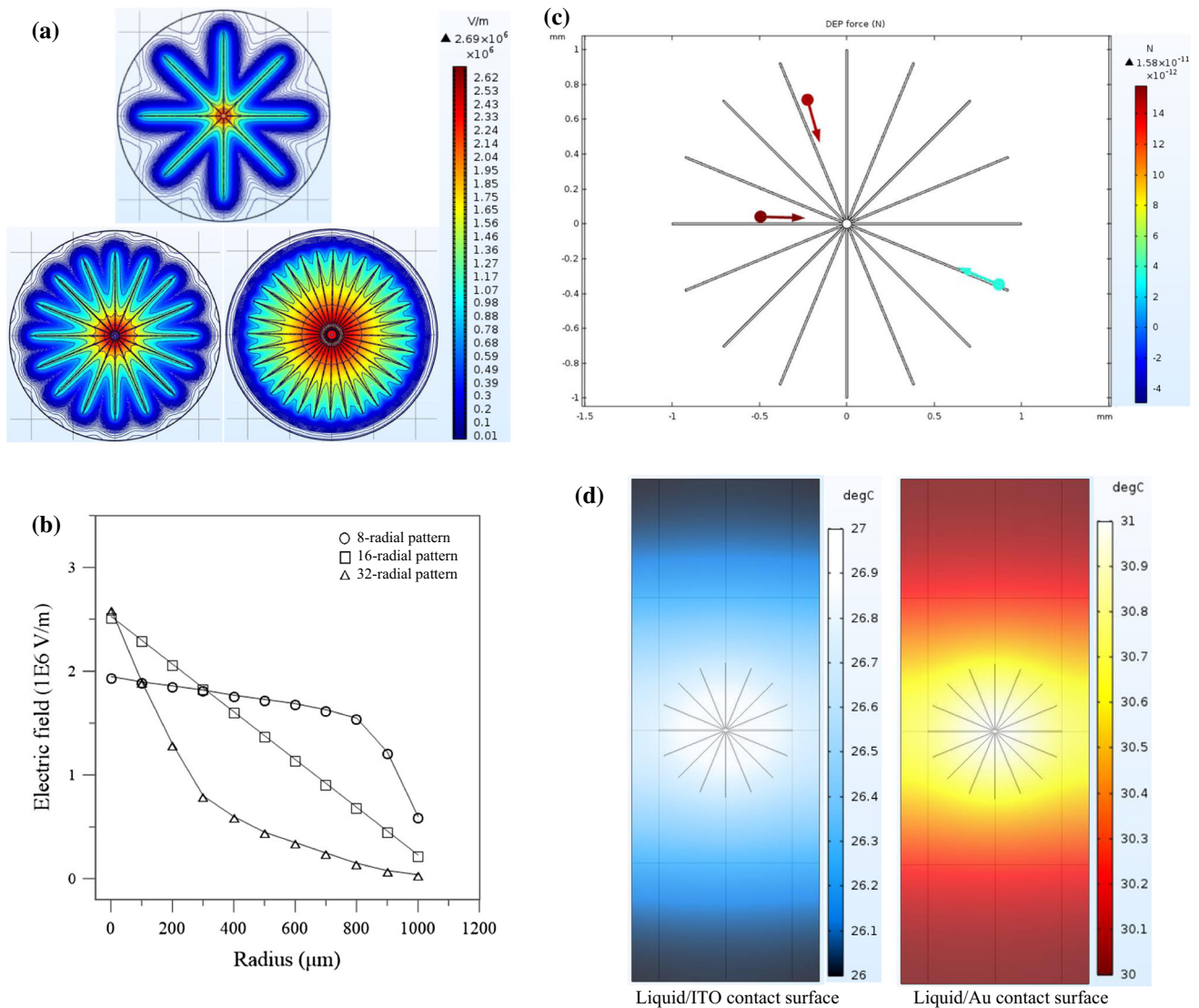
Fig. 3 Numerical simulation results for: **a** electrical field gradient (*Exy*) contours induced by three different radial patterns, **b** variation of electric field gradient over radius of virtual electrode, **c** DEP force for 16-radial pattern, and **d** temperature contours on liquid surfaces in contact with ITO layer (left) and Au film (right). (Note that electric field and driving frequency are 20 V$_{pp}$ and 300 Hz, respectively, in every case)

three projected patterns. For all three patterns, the electric field strength decreases with an increasing distance from the center of the pattern. Notably, the 16-radial pattern not only induces a high electric field strength (2.54×10^6 V/m) at the center of the projected image, but also exhibits a linear distribution of the electric field in the radial direction. It was thus selected for further numerical analysis and experimental investigation. Figure 3c shows the simulation results obtained for the positive DEP force vectors exerted on three 90-μm polystyrene beads trapped by the 16-radial pattern under an AC electric field of 20 V$_{PP}$ and a driving frequency of 300 Hz. As shown, the DEP force increases as the particle approaches the center of the radial pattern due to the corresponding increase in the

electric field strength. From inspection, the magnitude of the DEP force exerted on the particles ranges from several to more than ten pico-Newtons has been obtained by numerical simulations.

Due to the high thermal conductivity of the gold film (318 W/mK), the temperature also has an important effect on the behavior of the ODEP chip. When an AC electric field is applied to the ITO or gold surface, it heats the conducted area, which in turn heats the surrounding liquid. Previous studies have shown that the conductivity and permittivity of conductive fluids are both temperature-dependent (Mishra et al. 2014). Accordingly, the temperature distribution within the ODEP chip was evaluated using the COMSOL Multiphysics heat transfer module with thermal

conductivities of 0.75, 1.2 and 318 W/mK for the DI water, ITO layer and gold film, respectively. Figure 3d shows the temperature field distributions of the liquid surfaces in contact with the ITO layer (left) and gold film (right). For the considered electric field strength of 20 V$_{PP}$, the average temperature of the liquid layer in contact with the ITO surface is around 26.5 °C, and is thus only slightly higher than the assumed room temperature (25 °C). However, the average temperature of the liquid layer in contact with the gold surface is almost 31 °C. Furthermore, a small ($\sim$ 0.5 °C) difference is observed between the temperature at the center of the projected 16-radial pattern and that at the outside of the projected image.

4 Results and discussion

4.1 The electrolysis phenomenon and the ODEP device without gold nanofilm

Figure 4a presents a series of experimental observations showing the manipulation of a 90-μm polystyrene bead by a negative DEP force in a conventional ODEP device with no gold nanofilm. (Note that the electric field strength and driving frequency are 20 V$_{PP}$ and 30 kHz, respectively.) It is seen that the polystyrene bead is pushed away from the center of the radial pattern through a distance of 400 μm over a period of 60 s; corresponding to an average particle speed of 6.7 μm/s. A further series of experiments was performed using driving frequencies in the range of 100 Hz to 70 kHz. The corresponding results are shown in the upper panel of Fig. 5a. It is observed that a crossover frequency occurs at approximately 400 Hz. In other words, the particles experience a positive DEP force at driving frequencies lower than 400 Hz, but a negative DEP force at frequencies higher than 400 Hz. For an electric field strength of 20 V$_{PP}$ and driving frequencies less than 450 Hz, an electrolysis phenomenon is induced in the liquid layer of the ODEP chip, as shown in the inset of Fig. 4b. The resulting bubbles obstruct the manipulation of the particles. Consequently, in conventional ODEP devices (i.e. ODEP devices with no gold nanofilm), the manipulation of polystyrene beads immersed in DI water is restricted to negative DEP forces only (i.e., a one-directional operation ability) with driving frequencies greater than 450 Hz. Figure 4b illustrates the variation of the electrolysis frequency as a function of the driving voltage in the range of 16 $\sim$ 20 V$_{PP}$ for ODEP devices with and without gold films, respectively. It is seen that the electrolysis frequency is near linearly related to the driving voltage. In addition, the electrolysis frequency increases with an increasing nanofilm thickness.
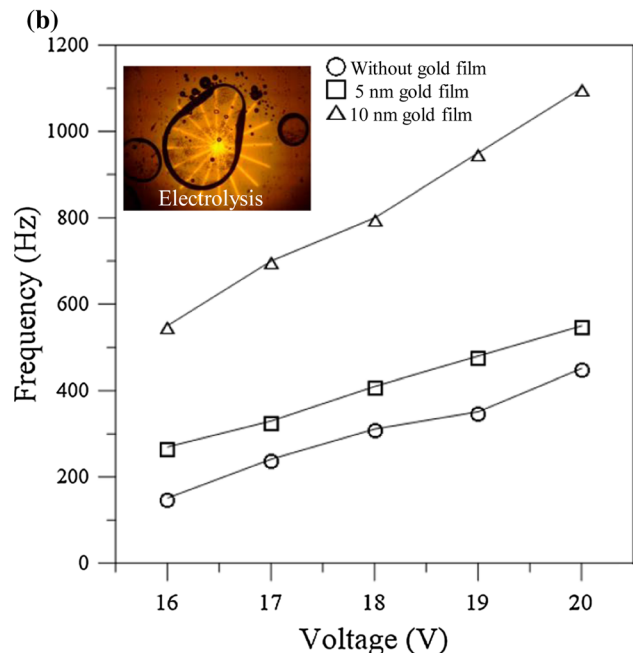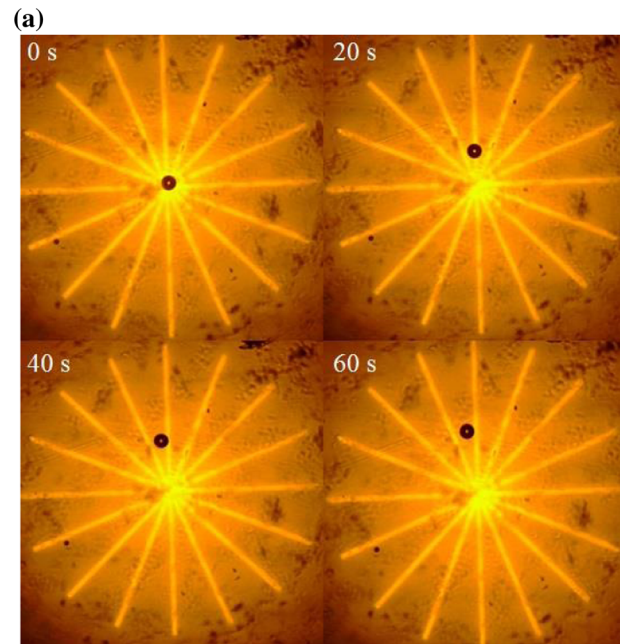
Fig. 4 a Experimental observations of particle manipulation by negative DEP force in ODEP device without gold film under electric field of 20 V$_{PP}$ and AC voltage frequency of 30 kHz. b Variation of electrolysis frequency with driving voltage as function of gold film thickness. (Inset shows the electrolysis phenomenon induced at driving frequency of 450 Hz for ODEP device without gold film under electric field of 20 V$_{PP}$)

4.2 The ODEP device with gold nanofilms

The middle and lower panels in Fig. 5a show the variation in the direction of the DEP force in ODEP chips incorporating gold nanofilms with thicknesses of 5 nm and 10 nm,
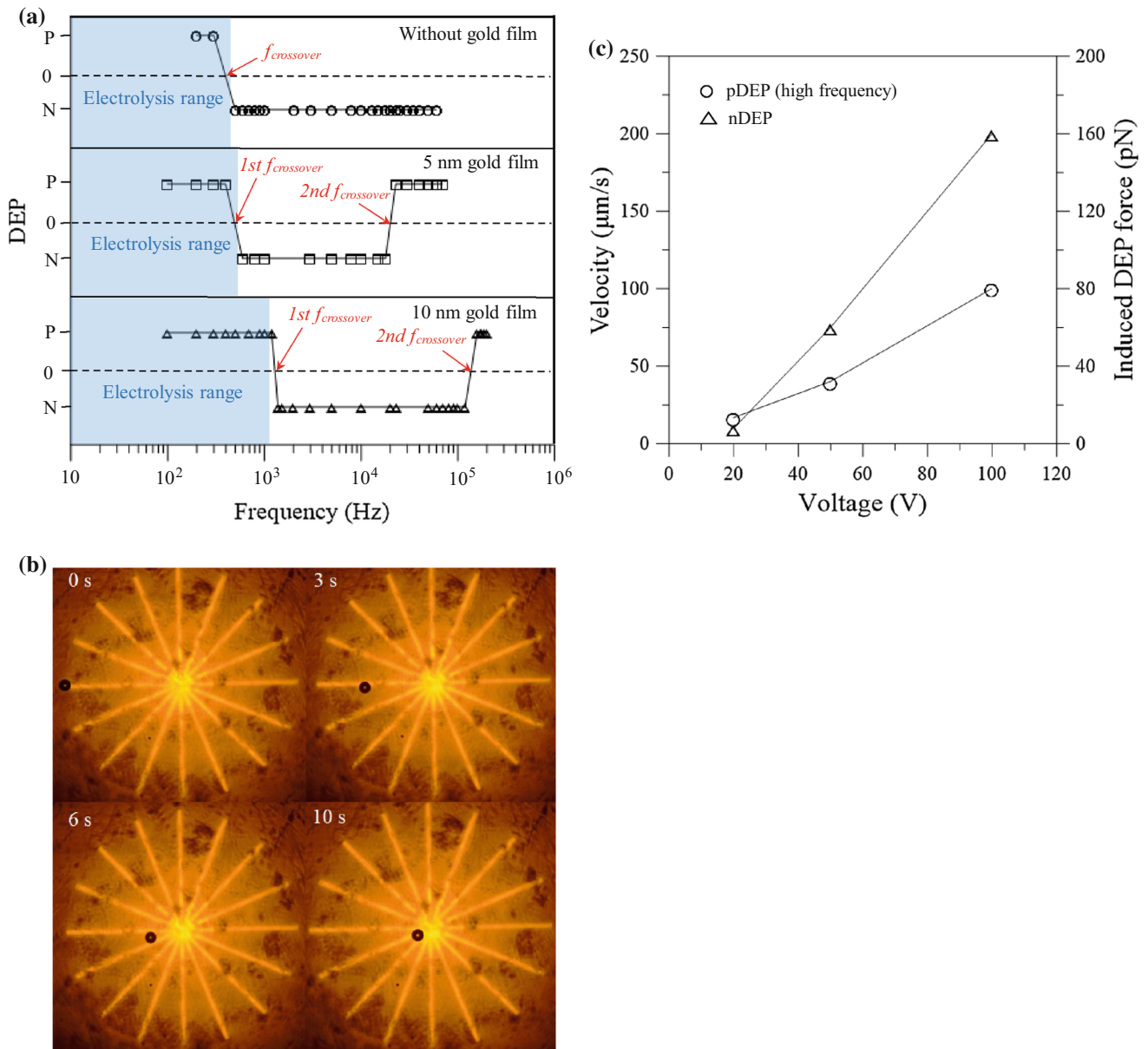
Fig. 5 a Experimental results showing variation of positive or negative DEP force as function of driving frequency in ODEP devices with and without gold film. **b** Experimental observations of particle manipulation by positive DEP force in ODEP device with 5-nm gold film under electric field of 100 V_{PP} and AC voltage frequency of 200 kHz. **c** Maximum manipulation velocity and ODEP manipulation force under different AC voltages

respectively, as the driving frequency is increased from 100 Hz to 250 kHz. (Note that the electric field strength is 20 V_{PP} in every case.) It is seen that, compared to the conventional ODEP chip, the inclusion of a gold nanofilm extends the useable frequency range of the ODEP device and introduces a second frequency crossover point at higher frequencies. For the ODEP device with a 5-nm gold film, the first crossover frequency and electrolysis frequency are located at 500 Hz and 550 Hz, respectively. By contrast, for the device with a 10-nm gold film, the electrolysis frequency and first crossover frequency are located

at 1100 Hz and 1150 Hz, respectively. For both devices, a positive DEP force cannot be used in the low frequency range due to the occurrence of electrolysis. However, as the frequency increases, a second frequency crossover point occurs at 20.5 kHz (5-nm gold film) and 140 kHz (10-nm gold film), respectively. In other words, the negative DEP force is replaced by a positive DEP force at high frequencies; indicating the feasibility for a bi-directional operation. In general, the occurrence of a second frequency crossover point indicates that the polystyrene particles are more polarizable than the medium (DI water) in the high

Table 1 Manipulation frequency and maximum particle velocity for ODEP devices with different gold nanofilm thicknesses

Gold nanofilm	Positive/negative DEP	Frequency (kHz)	Max. velocity (μm/s)
0 nm	Negative	30	6.7
5 nm	Negative	10	10
5 nm	Positive	50	16.7
10 nm	Negative	10	3.3
10 nm	Positive	180	6.7

Note that electric field strength is 20 V_{pp} in every case

frequency range. This phenomenon has been attributed to the electrothermal effect induced in high thermal conductivity media and the light absorption effect of the gold film (Wang et al. 2014). When an AC electric field coupled with light is projected onto the gold surface, a heating effect is induced in the illuminated area. This leads to a localized heating of the surrounding liquid, which produces spatial gradients of the conductivity and permittivity in the liquid medium. Consequently, the particles are driven toward the center of the virtual electrode.

Table 1 shows the manipulation frequency and maximum particle velocity in ODEP devices with different gold nanofilm thicknesses. Note that the electric field strength is 20 V_{PP} in every case. As shown, the maximum manipulation velocity (i.e., the maximum DEP force) is produced in the device with a gold nanofilm with a thickness of 5 nm. Notably, the device provides not only a negative DEP force at lower driving frequencies, but also a positive DEP force at higher frequencies. Consequently, it provides the ability to perform both particle concentration and particle separation on a single platform.

Figure 5b presents a series of images showing the manipulation of a 90-μm polystyrene bead by a positive DEP force in the ODEP device with a 5-nm gold nanofilm. Note that the electric field strength and frequency are 100 V_{PP} and 200 kHz, respectively. It is seen that the polystyrene bead travels in the inward direction through a distance of approximately 1000 μm within 10 s; corresponding to an average particle speed of around 100 μm/s. According to Stokes' law, the drag force acting on a spherical particle under continuous flow is given by

$$F_{st} = 6\pi a \eta v, \tag{4}$$

where a, η and v are the radius of the particle, the viscosity of the fluid, and the terminal velocity of the particle, respectively. According to Stokes' law (Eq. 4), the manipulation force acting on a particle can be assumed to be equal to the hydrodynamic drag force exerting on a moving particle. As a result, the manipulation force can therefore be experimentally estimated through the maximum manipulation velocity of a moving particle. In this study, experimental investigations were performed to determine the quantitative link between the manipulation

forces and the magnitude of electric voltage applied. For this purpose, the maximum velocity of a moving particle was experimentally measured to calculate the manipulation force based on Stokes' law.

Figure 5c shows the experimental results obtained for the maximum velocity and induced DEP force acting on the polystyrene beads in the ODEP device with a 5-nm gold film and driving voltages in the range of 20 ~ 100 V. For both a positive DEP force (pDEP) and a negative DEP force (nDEP), the results shown in Fig. 5c are in good agreement with the theoretical expression for the time-averaged DEP force in Eq. (1). In other words, the results confirm that the magnitudes of the maximum particle velocity and manipulation force are both proportional to the square of the applied driving voltage. This results also useful for the live and dead cells in the two cell species studied. Because of the DEP forces acting on the live and dead cells could be different. It was reported previously that the live and dead cells might experience positive and negative DEP forces, respectively, under the same operating conditions in which the exerted DEP force attracted the live cells but repelled the dead cells (Huang et al. 2014).

Overall, the results presented in Fig. 5 show that for an ODEP device incorporating a gold nanofilm, the direction of the DEP force can be controlled by adjusting the frequency of the driving voltage, while the velocity of the particles and the manipulation force can be controlled by adjusting the strength of the driving voltage.

5 Conclusions

This study has presented an ODEP device incorporating a gold nanofilm for microparticle concentration and separation purposes. The electric field gradient and DEP force induced by three different radial light patterns have been investigated by means of numerical simulations. It has been shown that a light pattern consisting of 16-radial spokes (16 virtual electrodes) not only produces a high DEP force, but also a linear distribution of the electric feld strength in the radial direction. The experimental results have shown that the inclusion of a gold nanofilm in the ODEP device increases the operating frequency range compared to that in

a conventional device with no gold nanofilm and induces a second crossover frequency point at higher frequencies. In other words, the device provides both a negative DEP force (at lower frequencies) and a positive DEP force at higher frequencies. As a result, the device can support both particle separation (at lower frequencies) and particle concentration (at higher frequencies) on a single platform. It has been shown that a gold nanofilm thickness of 5 nm results in an acceptable tradeoff between the electrical (conductive) and optical (transmittance) properties of the ODEP chip and produces the maximum ODEP driving force and particle velocity. Moreover, the DEP force and driving velocity can be controlled approximately linearly by adjusting the driving voltage. Overall, the results show that the proposed ODEP device provides a highly promising platform for sample separation and concentration in biomedical applications.

References

Chiou PY, Ohta AT, Wu MC (2005) Massively parallel manipulation of single cells and microparticles using optical images. Nature 436:370–372

Chiou CH, Pan JC, Chien LJ, Lin YY, Lin JL (2013) Characterization of microparticle separation utilizing electrokinesis within an electrodeless dielectrophoresis chip. Sensors 13:2763–2776

Chiou CH, Chien LJ, Lin JL, Kuo JN (2016) Novel electrodeless-dielectrophoresis device for nanoparticle trapping using three-dimensional inverted-pyramid arrays. Appl Phys Express 9:057001

Chu PY, Liao CJ, Hsieh CH, Wang HM, Chou WP, Chen PH, Wu MH (2019) Utilization of optically induced dielectrophoresis in a microfluidic system for sorting and isolation of cells with varied degree of viability: demonstration of the sorting and isolation of drug-treated cancer cells with various degrees of anti-cancer drug resistance gene expression. Sensor Actuat B Chem 283:621–631

Esseling M, Glasener S, Volonteri F, Denz C (2012) Opto-electric particle manipulation on a bismuth silicon oxide crystal. Appl Phys Lett 100:161903

Gascoyne PRC, Vykoukal JV (2004) Dielectrophoresis-based sample handling in general-purpose programmable diagnostic instruments. Proc IEEE 92:22–42

Gennari O, Grilli S, Coppola S, Pagliarulo V, Vespini V, Coppola G, Bhowmick S, Gioffré MA, Gentile G, Ambrogi V, Cerruti P, Carfagna C, Ferraro P (2013) Spontaneous assembly of carbon-based chains in polymer matrixes through surface charge templates. Langmuir 29:15503–15510

Grier DG (2003) A revolution in optical manipulation. Nature 424:810–816

Grilli S, Ferraro P (2008) Dielectrophoretic trapping of suspended particles by selective pyroelectric effect in lithium niobate crystals. Appl Phys Lett 92:232902

Grilli S, Coppola S, Nasti G, Vespini V, Gentile G, Ambrogi V, Carfagna C, Ferraro P (2014) Hybrid ferroelectric-polymer

microfluidic device for dielectrophoretic self-assembling of nanoparticles. RSC Adv 4:2851–2857

Huang Y, Yang JM, Hopkins PJ, Kassegne S, Tirado M, Forster AH, Reese H (2003) Separation of simulants of biological warfare agents from blood by a miniaturized dielectrophoresis device. Biomed Microdevices 5:217225

Huang SB, Liu SL, Li JT, Wu MH (2014) Label-free live and dead cell separation method using a high-efficiency Optically-Induced Dielectrophoretic (ODEP) force-based microfluidic platform. Int J Autom Smart Technol 4:83–91

Hughes MP, Pethig R, Wang XB (1996) Dielectrophoretic forces on particle in traveling electric fields. J Phys D Appl Phys 29:474–482

Hwang H, Choi YJ, Choi W, Kim SH, Jang J, Park JK (2008) Interactive manipulation of blood cells using a lens-integrated liquid crystal display based optoelectronic tweezers system. Electrophoresis 29:1203–1212

Hwang H, Lee DH, Choi W, Park JK (2009) Enhanced discrimination of normal oocytes using optically induced pulling-up dielectrophoretic force. Biomicrofluidics 3:014103

Jager EWH, Inganas O, Lundstrom I (2000) Microrobots for micrometer-size objects in aqueous media: potential tools for single-cell manipulation. Science 288:2335–2338

Jamshidi A, Pauzauskie PJ, Schuck PJ, Ohta AT, Chiou PY, Chou J, Yang P, Wu MC (2008) Dynamic manipulation and separation of individual semiconducting and metallic nanowires. Nat Photonics 2:86–89

Jamshidi A, Neale SL, Yu K, Pauzauskie PJ, Schuck PJ, Valley JK, Hsu HY, Ohta AT, Wu MC (2009) Nanopen: dynamic, low-power, and light-actuated patterning of nanoparticles. Nano Lett 9(8):2921–2925

Krupke R, Hennrich F, Lohneysen V, Kappes MM (2003) Separation of metallic from semiconducting single-walled carbon nanotubes. Science 301:344–347

Lu YS, Huang YP, Yeh JA, Lee CK (2006) Controllability of non-contact cell manipulation by image dielectrophoresis (iDEP). Opt Quantum Electron 37:1385–1395

Mello AJde, Beard N (2003) Focus. Dealing with 'real' samples: sample pre-treatment in microfluidic systems. Lab Chip 3:11N–19N

Merola F, Grilli S, Coppola S, Vespini V, Nicola SD, Maddalena P, Carfagna C, Ferraro P (2012) Reversible fragmentation and self-assembling of nematic liquid crystal droplets on functionalized pyroelectric substrates. Adv Funct Mater 22:3267–3272

Miccio L, Memmolo P, Grilli S, Ferraro P (2012) All-optical microfluidic chips for reconfigurable dielectrophoretic trapping through SLM light induced patterning. Lab Chip 12:4449–4454

Miccio L, Marchesano V, Mugnano M, Grilli S, Ferraro P (2016) Light induced DEP for immobilizing and orienting Escherichia coli bacteria. Opt Lasers Eng 76:34–39

Mishra A, Kwon JS, Thakur R, Wereley S (2014) Optoelectrical microfluidics as a promising tool in biology. Trends Biotechnol 32(8):414–421

Muñoz-Martínez JF, Ramiro JB, Alcázar A, García-Cabañes A, Carrascosa M (2017) Electrophoretic vs. dielectrophoretic nanoparticle patterning using optoelectronic tweezers. Phys Rev Appl 7:064027

Nasti G, Coppola S, Olivieri F, Vespini V, Pagliarulo V, Ferraro P (2018) On the complex and reversible pathways of CdSe quantum dots driven by pyroelectric-dielectrophoresis. Langmuir 34:2198–2204

Nguyen NT (2012) Special issue on magnetic-based microfluidics. Microfluid Nanofluid 13:527–528

Pethig R, Markx GH (1997) Applications of dielectrophoresis in biotechnology. Trends Biotechnol 15(10):426–432

Shi J, Huang H, Stratto Z, Huang Y, Huang TJ (2009) Continuous particle separation in a microfluidic channel via standing surface acoustic waves (SSAW). Lab Chip 9:3354–3359

Voldman J (2006) Electrical forces for microscale cell manipulation. Annu Rev Biomed Eng 8(1):425–454

Wang W, Lin YH, Wen TC, Guo TF, Lee GB (2010) Selective manipulation of microparticles using polymer-based optically induced dielectrophoretic devices. Appl Phys Lett 96:113302

Wang KC, Kumar A, Williams SJ, Green NG, Kim KC, Chuang HS (2014) An optoelectrokinetic technique for programmable particle manipulation and bead-based biosignal enhancement. Lab Chip 14:3958–3967

Yang SM, Yu TM, Huang HP, Ku MY, Hsu L, Liu CH (2010) Dynamic manipulation and patterning of microparticles and cells by using TiOPc-based optoelectronic dielectrophoresis. Opt Lett 35:1959–1961

Zhang S, Shakiba N, Chen Y, Zhang Y, Tian P, Singh J, Chamberlain MD, Satkauskas M, Flood AG, Kherani NP, Yu S, Zandstra PW, Wheeler AR (2018) Patterned optoelectronic tweezers: a new scheme for selecting, moving, and storing dielectric particles and cells. Small 14(45):1803342